Results in Engineering 19 (2023) 101373

Contents lists available at ScienceDirect

Results in Engineering

journal homepage: www.sciencedirect.com/journal/results-in-engineering

Heat transfer characterization with alternative heating element layout in electric 'Injera' baking technology

Anwar Endris Hassen [a,b,*], Lorenzo Pagliano [b]

[a] University School for Advanced Studies IUSS Pavia, Pavia, Italy
[b] end-use Efficiency Research Group, Department of Architecture and Urban Studies, Politecnico di Milano, Milan, Italy

ARTICLE INFO

Keywords:
Heating element
Heat transfer analysis
Thermal distribution
Energy efficiency
Clean cooking
Uniform heat distribution

ABSTRACT

The quantitative understanding of the heat transfer mechanism of injera baking technology is critical to evaluate energy consumption, cooking time, and thermal loss of the technology. However, the impact of the heating element layout on the heat transfer process has not been studied. Here, this paper studies four heating element layout arrangements consisting of a fixed power input with a varying power density as a function of layout design to investigate wiring layout impact on product performance. The conduction heat transfer of each heating element layout modelled using transient finite element simulation. Results indicate that higher power density bear a strong, positive correlation with startup time, which showed a 13% better performance when compared with the benchmark. The temperature distribution, however, incurs a 32% higher deviation. Whereas the model with the least favourable startup time shows a threefold higher performance than the benchmark. The results show wiring layout has influence over the key performance parameter of the technology.

1. Introduction

The latest world energy outlook report emphasises the global energy crises in the reported year could push over 100 million people back to using biomass for cooking [1]. Today, over half of the African population relies on wood gathering and agricultural and animal waste for cooking applications. The traditional use of this energy account for final energy use increased by over 40% between 2010 and 2019 [2]. To cope with the challenges, the development of efficient and clean cooking technologies with integration of renewable energy sources [3,4]has a critical role to play in energy democratisation in the developing world.

In a large part of Ethiopia, 82% of the population including 54% of the urban population, rely on solid biomass cooking fuel [5]. The traditional cooking setup is based on the use of biomass via processes with very low energy conversion efficiency of biomass. In Ethiopia, injera (flat bread from cereal teff) baking accounts for 85% of household energy use in urban areas [6]. Studies estimated the efficiency with which energy is used in the traditional setup of injera baking to be around 5–15% [7–10]. In addition, biomass usage for injera baking is associated with rapid deforestation and indoor air pollution [11–15]. Therefore, to introduce clean energy sources in the energy mix for the injera baking process, notable efforts made in the areas of solar, biogas, and electric baking technologies.

In research conducted by Hassen et al. [16] and Tesfay et al. [9], a new type of baking system powered by solar energy was proposed. The research also focuses on the integration of thermal energy storage in the baking system to bridge the mismatch between supply and demand. The proposed system introduces parts with a complex assembly process [17]. Therefore, the authors need to justify the economic strain of their proposed system as it requires higher capital costs and regular maintenance for its wide adaptation. Gallagher [18] also produced a solar-powered baking mechanism. However, the proposed setup only works for outdoor and sunny-environment applications, limiting its use.

In the biogas realm, research focuses on the development of a biogas burner that ensures uniform heat distribution to the baking surfaces [19,20], as heat distribution remains the major quality control parameter. Still, the thermal efficiency of the proposed biogas technologies remains a major concern as the provided air inlet can allow the escape of thermal energy. On the other hand, electricity-based injera baking technology demonstrated to be dependable and flexible in use. Simple in design and small components as shown in Fig. 1, allows the technology to be widely available in urban areas. The efficiency of the product ranges between 45 and 55% [17,21]. Even though the introduction of the electricity-powered injera baking technology dated back to the 1980s,

* Corresponding author.University School for Advanced Studies IUSS Pavia, Pavia, Italy.
E-mail address: anwar.hassen@iusspavia.it (A.E. Hassen).

https://doi.org/10.1016/j.rineng.2023.101373
Received 26 May 2022; Received in revised form 15 August 2023; Accepted 21 August 2023
Available online 25 August 2023

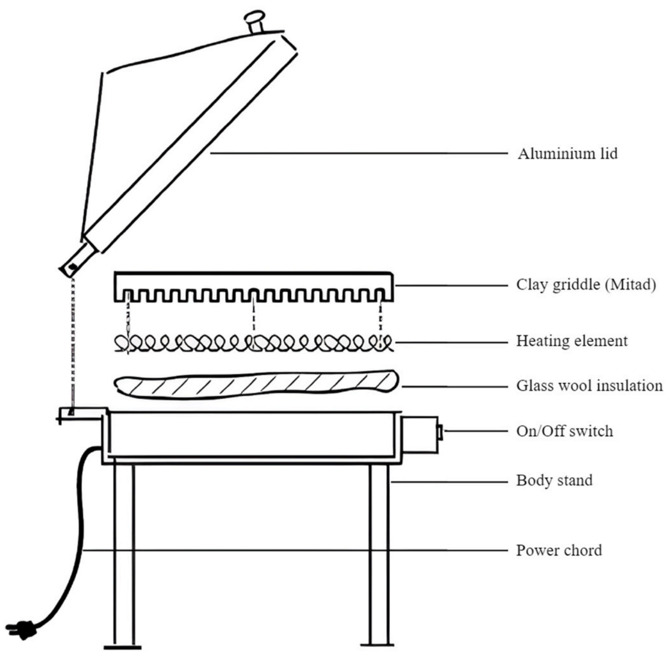

Fig. 1. Schematic overview of an electric injera baking technology [22].

there has not been any significant advancement documented. In 2016, the Ethiopian Standard Agency (ESA) and Ethiopian Energy Authority (EEA) established standards for locally produced electric injera baking stoves (ES ISO 04090:2016), and in 2020, a Voluntary Minimum Energy Performance Standard (MEPS) for the injera baking technology published. However, these standards have not yet been enforced and the manufacturing of the technology remains the same.

A typical locally manufactured electric injera baking technology requires a power input ranging from 3.5 kW to 4 kW [23], and the Ethiopian energy authority's 2015 report [24] projects the technology to reach over a million households in 2020. The estimation indicates the use of the technology has a significant strain on the power grid and indicates there is a need towards energy efficiency measures in the technology. After carefully examining all the available literature on the subject, the latest review article authored by Adem and Ambie [23] concluded that electric power injera baking stove technology is well established, and only requires an improvement in efficiency.

To improve energy efficiency in the technology, the literature concentrates on improving the thermal conductivity of the baking plate. Ceramics presented as an alternative to clay-made baking plates. Higher thermal conductivity and density of ceramics can allow the manufacturing of thinner baking plates for rapid heat transfer [16,25,22]. Another study [26], introduced new baking plate material which they claim to be more efficient, and the authors keep the thermophysical properties of the material confidential. Berhanu et al. [27] investigate copper powder as an additive material mixed with clay to manufacture a composite baking plate. Their study shows the additive manages to improve thermal conductivity by 62.4%. However, the effect of the proposed composite baking plates on the physicochemical parameters of the food remains unknown.

Researchers also employed numerical methods to facilitate the research to optimize injera baking operations' performance indicators. In Ayalew's PhD dissertation paper in 2009 [28], the Finite Element Method (FEM) was used for the first time in the subject area. Following the first attempt, similar studies conducted [29,30]. And the Finite Difference Method (FDM) was used in the study conducted by Awash in 2011 [25]. These studies share a similar objective where the baking pan alternative material thermal conductivity investigated. All the mentioned studies employed 2D transient simulation. However, after a careful examination of the injera baking problem and the baking technology, the 2D analysis used in the mentioned literature cannot address the problem. The 2D simulations do not resolve and consider the heat flow in the third (spanwise) direction nor the true asymmetrical heat load boundary condition, both of which can affect the heat transfer process.

In general, the technology has a small number of parts and requires no continuous maintenance. In most cases, the stove incurs a repetitive heating coil failure. A preliminary survey conducted for this study shows that a typical electrical baking stove could need an average of five heating coil replacements over its lifetime. The replacement process requires a total disassembly, hence, high maintenance costs. In all cases, the failure results from the formation of hotspots on the heating element. Hot spots on the heating element may result from uneven temperature distribution. Higher temperature concentrations at certain portions of the element will cause rapid oxidation of the heating element. Local oxidation reduces the cross-section of the heating element which in turn produces more heat locally and results in heating element breakdown. A

a) b) c)

Fig. 2. Heating element embedding process: a) Back side of clay plate with groove and resistor embedded; b) Sealed with gypsum; c) Plate dimension.

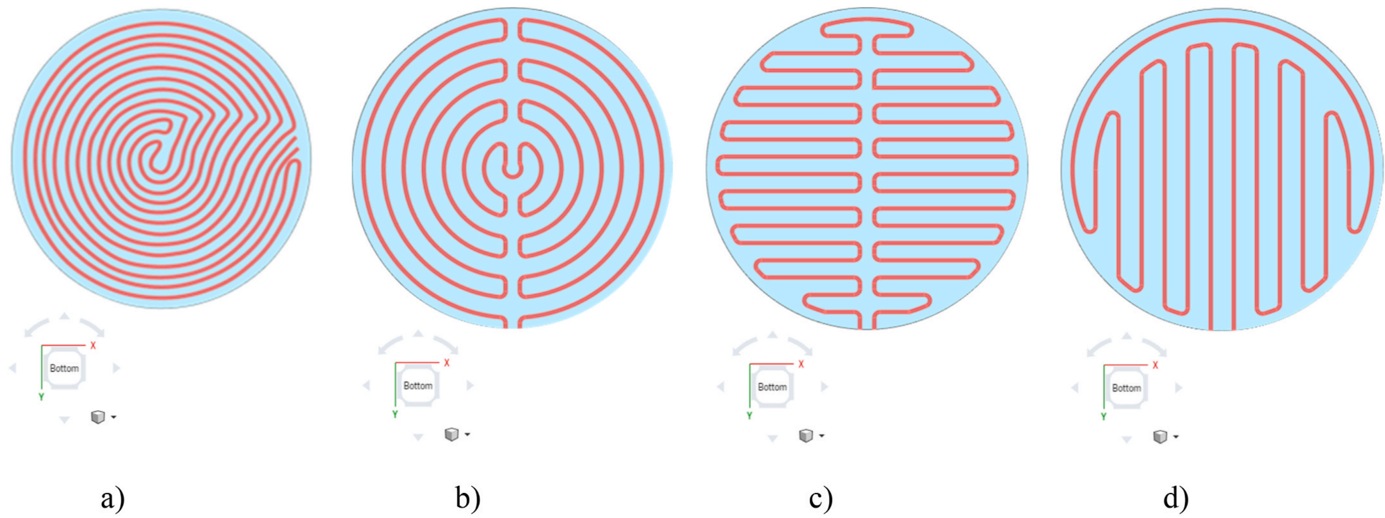

Fig. 3. Wiring layout design, the red part indicates heat load boundary condition: a) conventional wiring layout; b) model 1; c) model 2; d) model 3.

sharp and short pitch distance in the design of the heating element could exacerbate this problem.

To start the baking process, the baking surface needs to reach the baking temperature. Various pieces of literature propose 200 °C as an optimal temperature to start the baking process. The heat-up time of the baking plate depends on the power input, the thermal conductivity of the plate, the thickness of the plate, and the heating coil arrangement [27]. Depending on the factors, the heat-up time may range from 7 to 10 min. A shorter heat-up time can improve the baking cycle. The second parameter is temperature distribution on the baking plate. The baking plate has a wide surface area, therefore, uniform temperature distribution across the baking plate is required to avoid overbaking in certain portions of the plate. Mineral distribution in the clay used for manufacturing the baking pan and heating coil arrangement influence temperature uniformity on the baking surface.

Heating coil arrangement influence both performance indicators, however, there is no specific research work on the issue. Despite there is evidence that indicates the effect of wiring layout on the performance of injera baking technology we could not find any piece of literature dedicated to a quantitative understanding of the issue. Therefore, this study aimed to quantitatively understand the parametric relation the wiring layout has over the performance parameters through numerical analysis using four comparative models with different wiring layouts. The quantitative understanding of the effect will help to evaluate energy consumption, energy cost, cooking time, thermal energy loss, and heat transfer behaviour of the technology.

2. Materials and methods

The manufacturing of the technology involves three main steps. The first step is purely a pottery process where plastic clay moulded into a backing plate geometry. The clay plate has a high-quality smooth surface finish on the baking surface for waterproofing. The clay product then burnt at higher temperature for curing. Since there is no standard sizing of the baking plate, the dimensions may vary from one manufacturer to another and mostly range between 2.5 and 3 cm in thickness and between 50 and 60 cm in diameter [31]. The thermal conductivity of clay products is dependent on where the clay soil sourced which affects the mineral content of the soil type. Studies done by Geng and Sun [32] showed that the firing temperature also determines the product's thermal conductivity.

Next, after a quality check, the clay plate passes to electrical work. At this stage, the main objective is to embed the heating element in the baking plate. To do that, the backside of the clay plate grooved manually, and Fig. 2A present the final product. Because of the difference in thermal conductivity from plate to plate, the depth and pitch of the grooves are determined by studying the heating condition of the baking surface through trial and error. Therefore, the depth of the groove may vary between 1 and 2 cm. For heating purposes, the R09 nichrome resistor coil with a rated power of 1500 W used as a heating element. The R09 resistor has a standard length of 650 mm with a coil diameter of 6 mm. The heating coil has a helix structure with no pitch dimension when supplied. In the installation process, the wire stretched to increase its pitch, aiming to fit the length of the grooved space provided at the bottom of the pan. As the length of the grooved space increases, the coil also stretches to cover it. Based on the layout, the coil may stretch up to 12 *m*. The heating element then embedded in the groove as shown in Fig. 2A. In all cases, to achieve the length requirement with an acceptable power density and avoid overstretching, two heating coils used and connected in a series configuration. A plaster gypsum used to seal the heating element in the grooved area as presented in Fig. 2B. The gypsum layer will have a maximum of 1 mm of thickness off from the bottom side of the baking clay pan and the layer serves as an electric insulation material [31]. The final stage involves the outer bodywork, which has no relevance to the heat transfer process.

2.1. Simulation setup parameters

2.1.1. Geometrical modelling

In this study, the conventional wiring layout will serve as a benchmark for the parametric study of three newly proposed wiring layouts. To prepare the CAD model, the study followed up with the manufacturing process of a single baking stove. Fig. 2a shows the backside image of the case baking pan after the groves are prepared and the resistor embedded. The image used as a direct reference to trace the heating element path in the CAD software. Fig. 2b shows the backside of the plate sealed with gypsum and all the necessary dimensions of the baking plate are shown in Fig. 2c. The case baking plate has a 0.56 *m* diameter and a thickness of 0.025 *m*. The top surface has an effective baking surface diameter of 0.52 *m*, circled with a 0.02 *m* higher notch that aims to keep the batter inside the effective baking area. On the bottom, the groove path is directly traced from the image as shown in Fig. 2b, and the case model has a groove depth of 0.012 *m* and a pitch distance of 0.01 *m*. Thus, there is a 0.013 *m* effective distance between the baking surface and the heating medium. The plaster gypsum has an effective thickness of 0.002 *m* from the bottom surface of the plate.

The main drawback observed from the conventional wiring layout (shown in Fig. 2) is that the layout design has a small pitch distance and sharp turns. As discussed in the early section, this could result in heat spots that result in rapid oxidation of the heating element on turning corners. On the other hand, if a wider space is used, the heat distribution uniformity on the baking surface could be affected. Hence, when proposing a new wiring layout, the smallest distance that can allow a minimum of 0.01 *m* radius is presented as an acceptable turn radius to avoid the formation of hotspots. After experimenting with the CAD model, the ample gap was identified to be 0.03 *m* and used in the wiring layout design of Model 1 and Model 2 shown in Fig. 3. Whereas, Model 3 has a 0.04 *m* pitch distance. The use of different pitch distances will result in different contact surface areas that influence the power density of the design. All CAD models are presented in Fig. 3.

2.1.2. Thermophysical property

The use of refractory material in high-temperature cooking applications has the advantage of higher resistance to temperature-induced wear. This property gives the product a longer life cycle. The numerical analysis of a heat transfer problem can be treated using heat diffusion equations. The heat diffusion equation requires the density (ρ), specific heat (Cp) and thermal conductivity (k) variables. These variables in the current proposed problem require an experimental measurement of the clay material and the sealing gypsum plaster. Despite different constraints that come into play to determine the thermophysical property of the clay plate, surprisingly three research conducted independently reported near similar values. A study conducted by Awash [25] and Getenet [29] reports clay property values $\rho = 1900$ kg/m^3, Cp = 835 J/kg and K = 0.5 W/m^2. The latest paper on the topic [27] also reports Cp = 790 J/kg and K = 0.5 W/m^2. Therefore, in the current study, the average value of the reported experimental values was used to get representative data to characterise the thermophysical property of the clay plate for numerical analysis.

Gypsum plaster has a wide application in different construction applications worldwide. As a result, there are different studies scrutinising its property under different conditions and the thermophysical properties are different across the literature. Therefore, for the current study, the thermophysical properties needed to define the gypsum material in the simulation were taken from the literature [33,34]. The literature highlights that the density and thermal conductivity of the gypsum plaster is highly dependent on temperature. In that regard, as the baking stove is expected to work between the temperature ranges of 150 and 200 °C, the average value of the required parameter ($\rho = 836.4$, Cp = 950, and k = 0.25) is used as in the specified temperature range.

2.1.3. Boundary condition

SimScale with Code Aster solver is used to perform transient heat transfer analysis. During operation, the heat transfer process can be analysed as follows: When the electric resistors, embedded in the baking pan, are powered, the coil will generate a heat flux. The heat flux is the ratio of the resistor power and the heating element surface area, also known as wattage (watt density) shown in Equation (1). Embedded heating elements have direct contact with both the baking plate and the sealing material. Thus, the generated heat flux transfers through conduction, reaching all corners of the product as a vector quantity. Based on this analysis, the conduction heat transfer analysis type was selected to solve the problem. Conduction heat transfer treated using Equation (2). To account for the time-variant effect of the transfer phenomena, Equation (3) treats the problem as transient heat diffusion [34]. The thermophysical properties needed to solve the system problem are defined in the early section.

$$Watt\ Density = power / \ surface\ area \tag{1}$$

$$\frac{q}{t} = \frac{kA\, dT}{d} \tag{2}$$

Table 1
Watt density of the heating element layout design.

Configuration	Baseline	1	2	3
Rates Power (W)	3000	3000	3000	3000
Length of grooved space (m)	11.13	6.912	7.42	5.96
Heat source contact area (m^2)	0.21	0.13	0.14	0.11
Surface heat flux (W/m^2)	14299.25	22995.02	21458.66	26891.05

$$\frac{\partial^2 T}{\partial x^2} + \frac{\partial^2 T}{\partial y^2} + \frac{\partial^2 T}{\partial z^2} + \frac{q}{k} = \frac{\rho c_p}{k} \frac{\partial T}{\partial t} \tag{3}$$

Where q represents heat transfer (w); t represents time (s); k represents thermal conductivity; A represents heat transfer area (m^2); d represents material thickness (m); dT = T_1-T_2 represents temperature gradient (°C); ρ represents density (kg/m^3); Cp represents specific heat (J/kg K).

The heat transfer problem, in the current problem, has three main parts which are the heating element as the heat flux generator, the clay baking pan, and the sealing gypsum plaster. The configuration of the heat transfer parts allows no relative displacement between two connected solid bodies, hence, the contact between parts is defined as "bonded contact" in the simulation setup. Following contact definition, the initial condition of the problem is defined as the global temperature of the system being at 20 °C. Next, the heat flux load of the system is applied as the only boundary condition. The heat load can be applied as a fixed temperature or as a surface heat flux. The problem heating element is known; therefore, the power/watt density of the problem can be calculated using Equation (1).

Direct usage of Equation (1) will give a similar power density for all cases as a boundary condition. However, direct use of the formula can fail to define the heat flux distribution across the given heat transfer system and does not define the relationship between the heating element and heat-receiving parts. In such a case, the author proposes to define the power density of the system as a function of contact surface area instead of the area of the heating element. The definition of power density as a function of element wattage and contact surface area between the heating element and both the plate and gypsum helps simplify the model.

The proposed function allows the direct application of boundary conditions as surface heat flux on the contact surface area without the need to model the heating element, reducing the CAD model into two parts. The heating medium has a direct heat load on both the clay plate and the sealing gypsum; therefore, the contact area is measured as both the surfaces of the baking plate and the sealing gypsum. The element wattage remains constant in all models as a controlled parameter of 3 kW. Therefore, the surface heat flux load applied in the simulation for each model is defined as the ratio of power input of the heating element divided by the contact surface of the baking plate of each model. The surface heat flux of the heating element is calculated, and the results are shown in Table 1 for each case and applied to highlighted areas in Fig. 2, with their respective value.

2.2. Record keeping and performance analysis parameters

As indicated earlier, in this study three performance parameters were used to conduct a cross-model comparison while using the result from the conventional design as a benchmark. The three parameters are heat-up time, heat uniformity, and efficiency. This section discusses the record-keeping mechanism employed to measure the required parameters in the computational environment for a given performance indicator of the technology.

2.2.1. Startup time

The startup time tells us the duration it takes for the baking floor to reach a baking temperature from the surrounding temperature. The baking temperature is widely accepted to be around 200 °C, in a

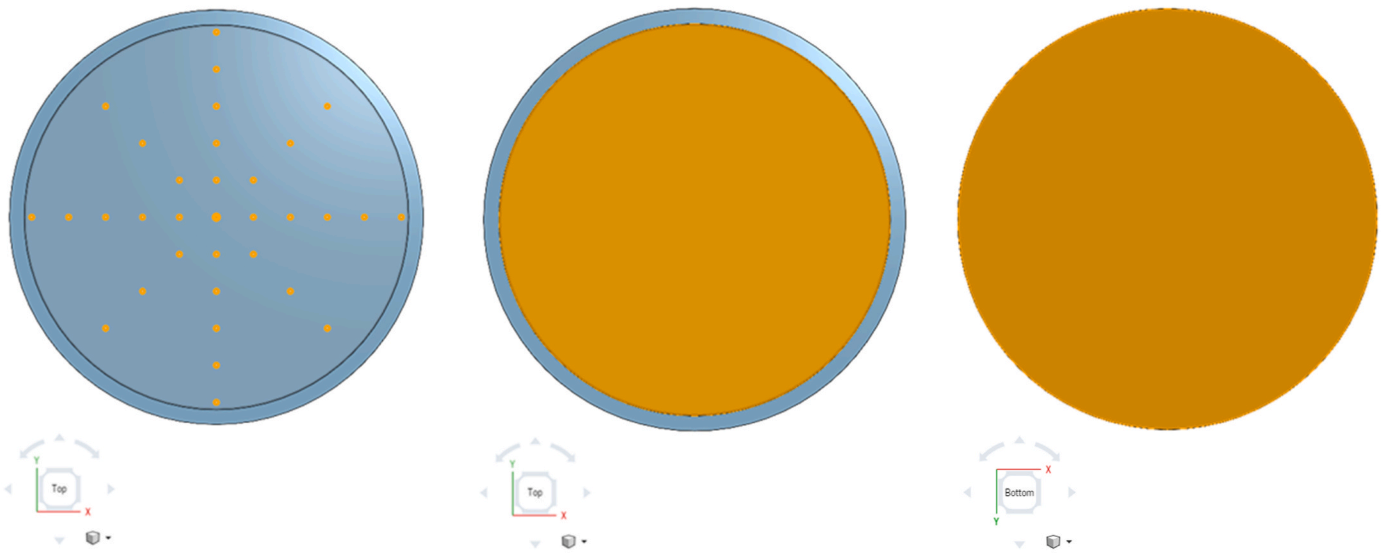

a) b) c)

Fig. 4. Recording keeping a) point temperature data collection; b) baking surface heat flux recording; c) non-baking surface heat flux recording.

temperature range that can vaporise water content in the batter. A shorter heat-up time would allow for the early commencement of the baking process and fast baking surface temperature recovery between the baking cycles. This will increase the total productivity of the process. The temperature value calculated over the mesh nodes presented on the surface of the baking floor is shown in Fig. 4b over the solution time. Both the maximum and minimum temperatures were solved on the baking surface. The average temperature distribution of the baking surface was also included in the result control parameter. The maximum and minimum temperature spots can be located using a colour map of the result and the average temperature was used to determine the heat-up time.

2.2.2. Temperature distribution

As indicated in the introduction section, temperature uniformity across the baking surface has a direct relationship with product quality. To investigate temperature uniformity, the temperature data were recorded on proposed measuring points over the transient time and standard deviation was used as a method of statistical analysis of the result [18]. highlighted that special attention should be given to the temperature data measurement spot at the baking surface and recommends a symmetric arrangement of the measuring points in eight dominant directions shown in Fig. 4a, and this study adopted the recommended arrangement to place the measurement points. To supplement the result discussion, the colour-mapped temperature distribution results of the baking surface were used for graphical inspection.

2.2.3. Thermal performance

Finally, the concept of efficiency in an injera baking stove differs across the energy inputs. In the case of electric baking technology, both thermal and electrical terms are used to calculate efficiency. Equation (4) presents a general term that is widely used to calculate energy efficiency. The technical and performance requirement for household single plate resistor-based electric injera baking stove draft standard (ES ISO 04090:2016) introduced Equation (5) to determine the energy efficiency of injera baking technology. The introduced formula encompasses operational parameters to calculate efficiency. However, when employing numerical methods for product optimization, such as the current study, does not necessitate the operational parameters to evaluate performance. Therefore, it was found essential to introduce a new performance evaluation method for the current study objectives.

$$\eta = \frac{Total\ Energy\ utilised}{Total\ Energy\ Input} \times 100\% \tag{4}$$

$$n_{th}(PHU) = \frac{K_w m_b C_{pw}(T_b - T_{iba}) + m_e L_v + K_f m_b C_{pf}\ (T_{ba} - T_{iba})}{Input\ power\ (Amps\ x\ volts\ x\ 3.6)} \times 100\% \tag{5}$$

Where $n_{th}(PHU)$ is the baking technology thermal efficiency, c_{pw} represents specific heat capacity of water, C_{pf} represents specific heat capacity of teff flour, L_v represents latent heat of vaporisation of water, K_w represents water fraction in the batter, K_f represents flour fraction in the batter, T_b represents water boiling point, T_{iba} represents the initial temperature of batter, T_{ba} represents baking temperature, m_b represent the mass of batter, m_e represents the mass of water evaporation.

To bridge the gap, the presented study introduces additional performance characterization concepts in the baking technology from a numerical analysis standpoint. In the early section of the study, the operation of the baking technology was analysed. From the analysis, it can be understood that there are two main heating phenomena in the technology operation. Since heat flux is a vector quantity, the transfer phenomena occur in all directions of the baking pan, towards the baking area, Fig. 4b, and to the non-baking area of the plate, shown in Fig. 4C. In a numerical setup, the value of heat flux can be calculated at a specific area of interest. Therefore, a ratio between heat flux values measured at baking and non-baking surface as they happen simultaneously could give needed insight into the technology performance.

$$\frac{Q_{bs}}{Q_{nbs}} \tag{6}$$

Based on that, Equation (6) was proposed as a performance evaluation of the baking technology defined as flux ratio, where Q_{bs} indicated the heat flux to the baking surface and Q_{nbs} indicated heat flux to the non-baking surface. A similar performance analysis approach is used to determine aerofoil performance in different industries. From the relation, it can be understood that a higher flux ratio indicates better performance of the system. To help record the desired quantities, two result control parameters are employed. The baking surface average heat flux result control applied to the surface is shown in Fig. 4b, while the non-baking surface heat flux control parameter applied to the surface is shown in Fig. 4c.

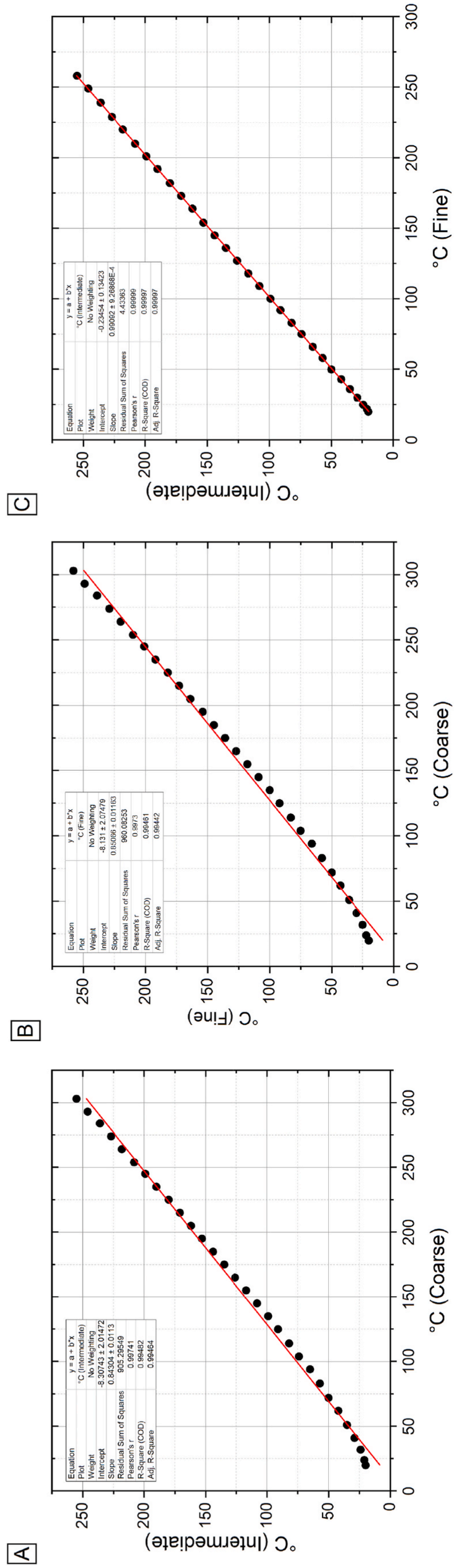

Fig. 5. Comparison of temperature value: (A) Coarse–Intermediate grids, (B) Coarse–Fine grids, (C) Fine–Intermediate grids.

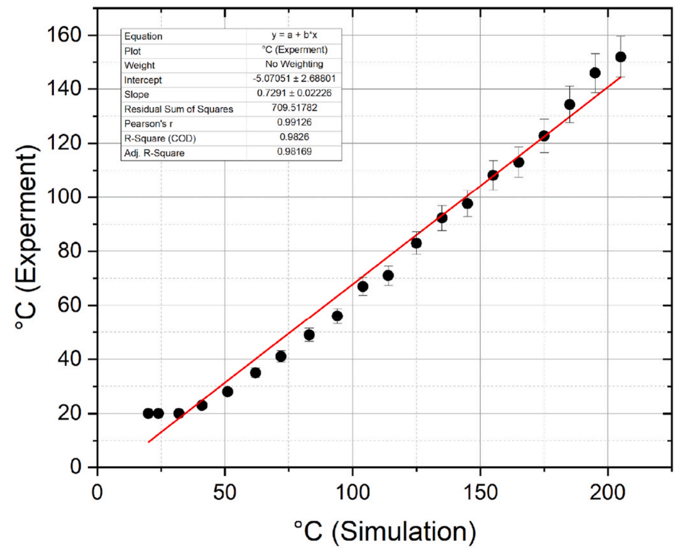

Fig. 6. Comparison of temperature value from experiment and numerical simulations.

3. Accuracy of the numerical simulation

3.1. Mesh independency test

Prior to the heat transfer simulation, a grid independence study was conducted over three grid resolutions. For this purpose, the geometrical model of the conventional wiring layout was used. The heat transfer occurs between the heating element and the baking plate contact area; therefore, a particular effort was made by adding surface refinement to ensure the contact surface has higher mesh quality. In this study, with a fixed grid ratio of 0.5, three computational meshes were prepared with a mesh size of 500 K, 1 M, and 2 M cells.

For a comparative study, the average temperature of the baking surface was recorded for every 30s intervals of the 900s simulation time step. A transient heat transfer simulation was conducted for all three cases with similar boundary conditions discussed in the early section. The result of the numerical calculation is presented in Fig. 5. The average temperature value of the coarse mesh size and the intermediate mesh size recorded a coefficient of divergence (R^2) value of 0.994, which is lower than the tolerance value of 1%. A similar R^2 value is also obtained when the result of the coarse mesh is compared with the fine mesh size as shown in Fig. 5B. The final figure shows the comparison result of moderate and fine mesh size and a remarkable R^2 value of 1 obtained, exhibiting there is no result dependency resulting from the cell size difference. Considering computational efficiency, the mesh generation setup used to generate the intermediate mesh size was adopted for further simulation conducted in this study.

3.2. Model validation

Because of the absence of comprehensive experimental studies recognizing the current study objective, experimental results were needed to adequately validate the numerical accuracy. First, a production of the baking technology with a conventional wiring layout was followed at the host production enterprise. After the compilation of the technology production, a test run was conducted on a case clay pan shown in Fig. 2. Using a non-contact infrared thermometer, the temperature at the centre of the clay baking plate was measured for 600s with 30s intervals. The experiment was conducted following a test procedure outlined in a technical standard (ES ISO 04090:2016).

At the beginning of the measurement, the surrounding temperature was recorded at 18.7 °C. For calculation purposes, the author proposed

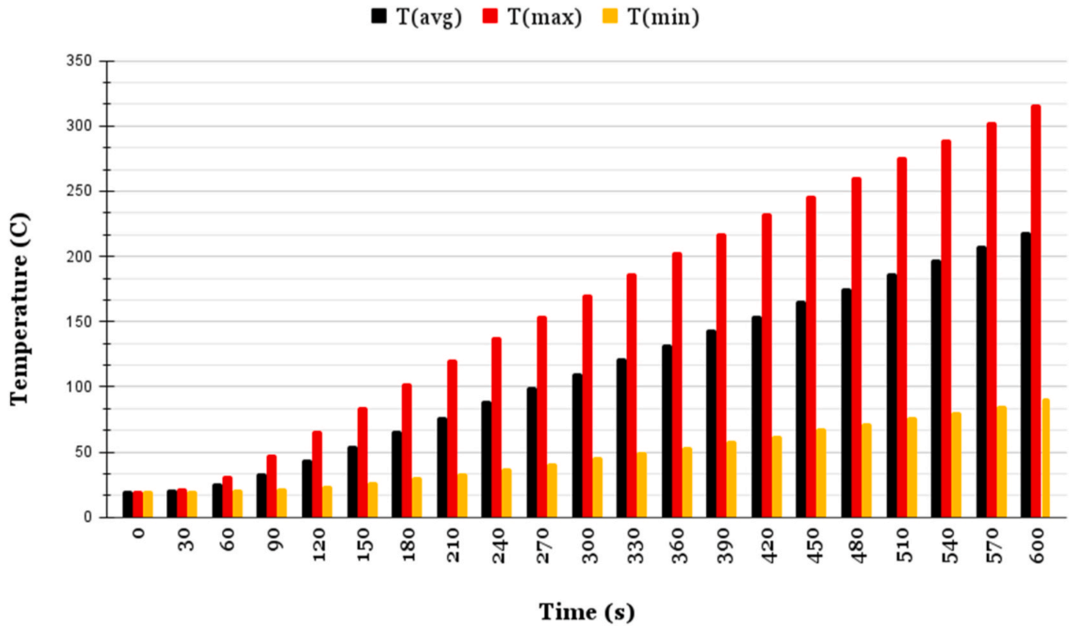

Fig. 7. Temperature record on the baking surface.

that the initial global temperature be set at 20 °C after the power supply. To achieve the desired initial temperature, the baking stove was preheated to 20 °C through continuous monitoring of the temperature at the proposed centre point of the pan before beginning the record keeping. The record-keeping was conducted manually by registering the value on a timesheet. After the temperature of the baking surface was calibrated, the record-keeping continued for the proposed period, and the calibrated temperature was considered as the initial time step. A temperature comparison between the experiment and the recorded data was used to evaluate the accuracy of the numerical result.

In the computational model, the simulation is set up following the parameters discussed in section 2.3 using the conventional wiring layout geometrical model shown in Fig. 2b depicting the exact geometrical feature as that of the experimental baking plate. The probe point at the centre of the geometrical model shown in Fig. 5a proposed to record the numerical temperature value with a similar time interval as that of the experiment. This allows the generation of a similar data set with the experiment result that can be directly compared. Fig. 6 compares the temperature value in the numerical simulation and the experimental test of the baking pan. In general, the temperature value obtained in the numerical simulation is lower than the corresponding temperature in the experimental test with a larger deviation at the start and final stage of the record keeping. A good agreement was found in between. The deviation may occur from external environmental effects in the experimental setup that the simulation setup does not consider. Nonetheless, the root mean square error of approximation between the experimental and numerical temperature result is 0.022 showing a good fit.

4. Results

The result section was divided into two parts. In the first section, the baseline study performance result was presented whereas the second section presents all three newly proposed wiring layout performances. The result of the three performance parameters of the case models is presented in each own subsection.

4.1. Baseline study

The three performance parameters that this study investigates are heat-up time, temperature distribution and efficiency. In action to point data of the temperature distribution results, a graphical inspection of the heat distribution on the baking surface was also presented.

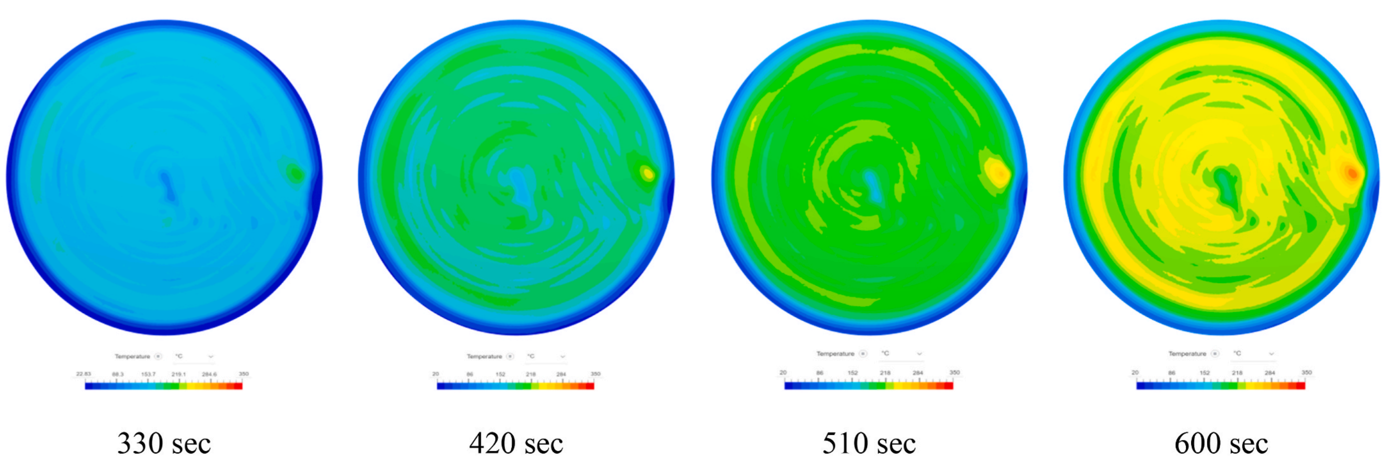

Fig. 8. Temperature distribution on the baking surface.

Table 2
Summary of temperature measurement on the probe points for conventional wiring layout.

Baseline model		Temperature (°C)			
Observation points	Time step (s)	Mean	Std. Dev.	Maximum	Minimum
33	60	42.3	10.6	59.0	22.0
33	150	77.3	13.0	99.0	36.0
33	240	112.1	14.9	139.0	58.0
33	330	146.0	16.7	176.0	83.0
33	420	179.4	18.4	209.0	109.0
33	510	212.4	20.0	242.0	136.0
33	600	245.1	21.7	278.0	164.0

4.1.1. Heat-up time

The heat-up time for the current study was accepted as 200 °C. As highlighted in the early section to help measure the heat distribution simulation result at the baking surface, a result control parameter was used, and the result is presented in Fig. 7. The horizontal axis represents the simulation time value where the result is recorded, and the vertical axis shows the corresponding temperature value recorded at the baking surface. The result shows there is uneven temperature distribution on the baking surface which will be discussed in the next subsection.

For comparison observation, the maximum and minimum temperatures recorded at the baking surface are plotted on the graph. The linear trendline analysis of the three temperature values in the plot shows an upward trend where the maximum temperature (T_{max}) has an increasing trend slope of 15.7 and the minimum temperature (T_{min}) on the baking surface has a 3.77 increasing trend. The conventional wiring layout average temperature (T_{avg}) distribution on the baking surface passes the acceptable baking temperature of 200 at 570s, establishing the design heat-up time.

4.1.2. Temperature distribution

Fig. 8 presents the colour-mapped temperature distribution result of the conventional heat coil layout on the baking surface for four representative solution times of 330, 420, 510, and 600 s after the power supply is initiated. Graphical inspection of the numerical result can help identify the potential cold and hot spots on the baking surface. As the time step increases, the temperature at the baking surface increases revealing both the hot and cold spots on the surface. The colour map result is scaled linearly to illustrate a temperature range between 20 and 350 °C.

The colour-mapped result shows that the layout design creates a cold spot at the centre of the baking plate. The wiring layout also has a hot spot at the edge of the pan. The review of the layout design shows at the middle of the plate the pitch distance of the heating element is larger. This creates a cold spot as observed. Whereas the hot spot occurred because of a small heating coil pitch gap. The graphical inspection of the colour-mapped result illustration highlights the cold and hot spots of the wiring layout design. To have a better quantitative understanding of the temperature distribution, the recorded temperature at the 33 measuring points, Fig. 4a, was analysed to draw a statistical relation.

The result presented in Table 2 and only seven of the total 32 solution time presented in the table. The standard deviation of the temperature result on the 33 locations shows a 13% increase in average for every 90s increase in the solution time. However, as the temperature increases with a direct relation to the solution time, the standard temperature deviation recorded on the location tends to decline. This shows the conventional wiring layout has better temperature uniformity across the baking surface at a higher working temperature.

4.1.3. Thermal performance

The applied boundary condition has a surface flux property, and the transport phenomena in the system defined by the thermophysical properties of the material determine the system energy performance. The applied surface heat flux has a fixed value that is not time dependent. The applied heat flux spontaneously flows along the temperature gradient between the heating element and the baking plate. In the presence of a constant supply of heat flux from the heating element, the temperature will increase over time as shown in Fig. 7 on the baking surface. However, heat flux on the other hand, implied by the energy conservation principle that is dictated by the first law of thermodynamics, remains constant once the optimal transfer is reached.

Therefore, as the solution time increases, the heat flux value is expected to reach thermal equilibrium. This indicates the system's ability to transfer the applied heat flux in the desired direction defines the system's performance. Fig. 9 plots the average heat flux value recorded on both baking surface and non-baking surfaces indicated in Fig. 4b and c. In the graph, the black bar indicates the average heat flux value that

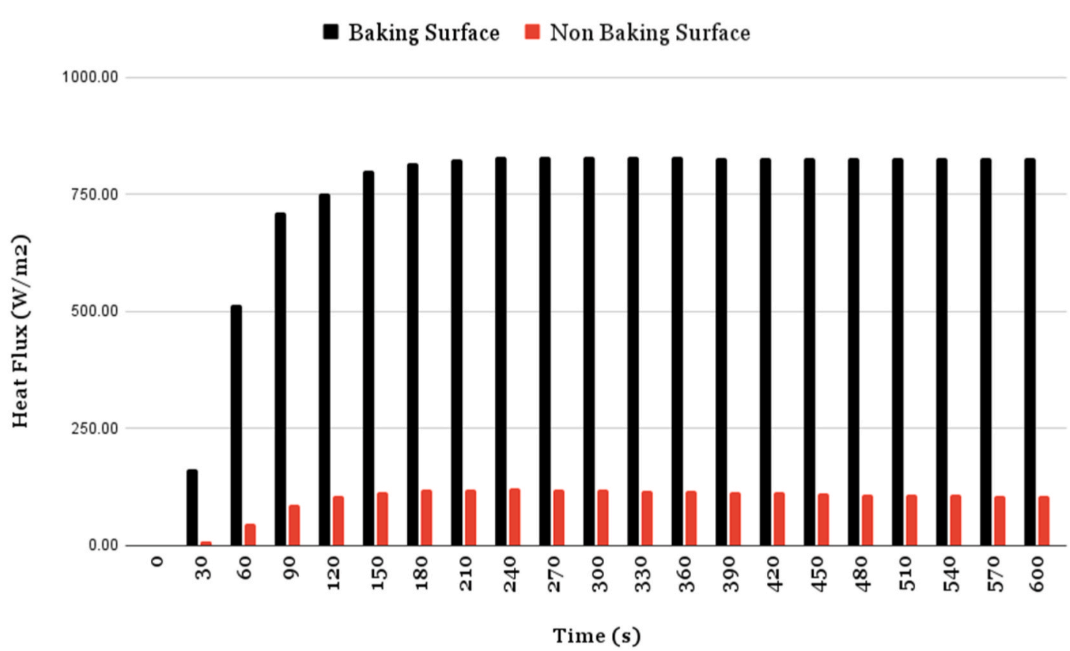

Fig. 9. Heat flux delivery to the baking surface and non-baking surface.

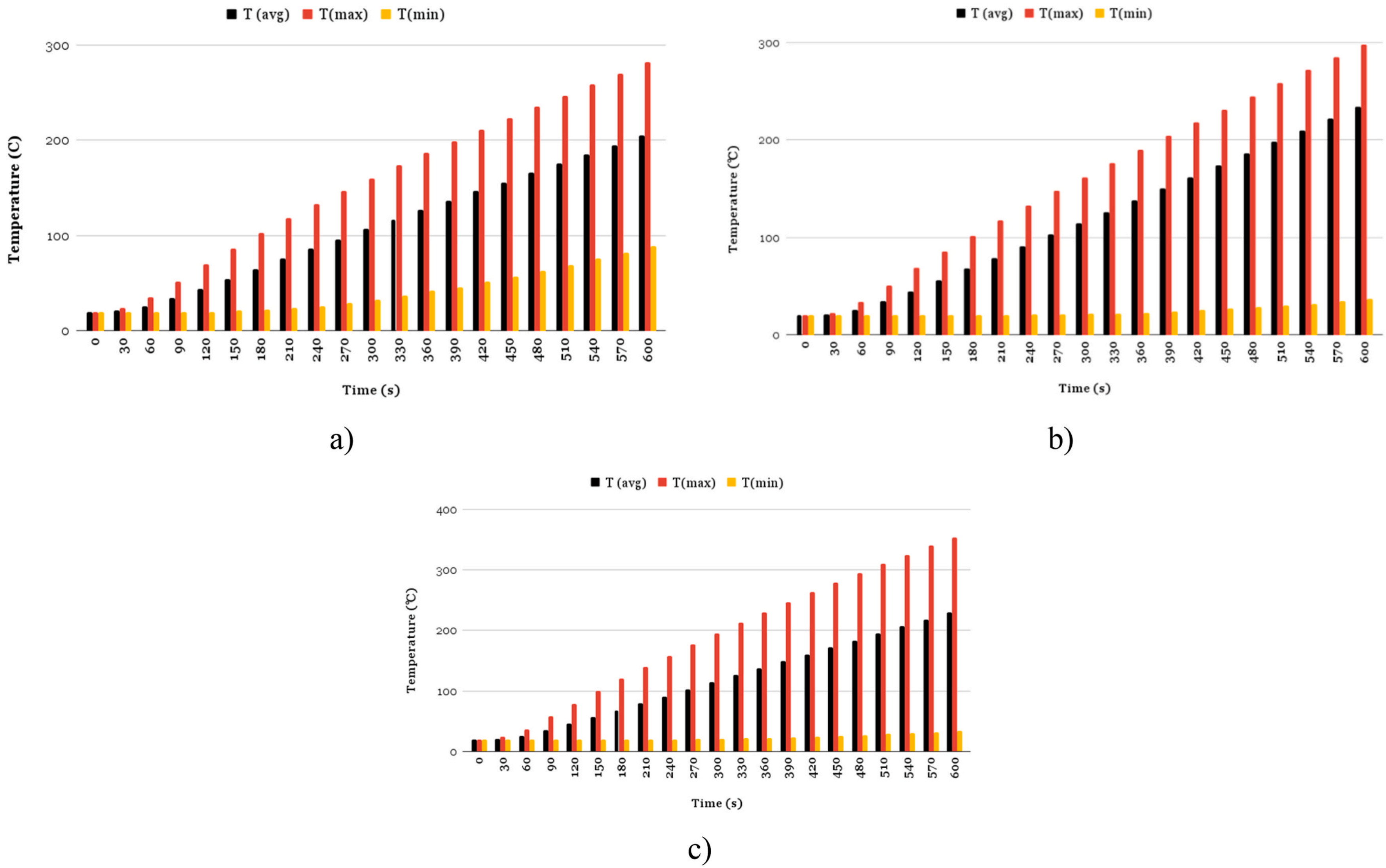

Fig. 10. Temperature recording on the baking surface: a) model 1; b) model 2; c) model 3.

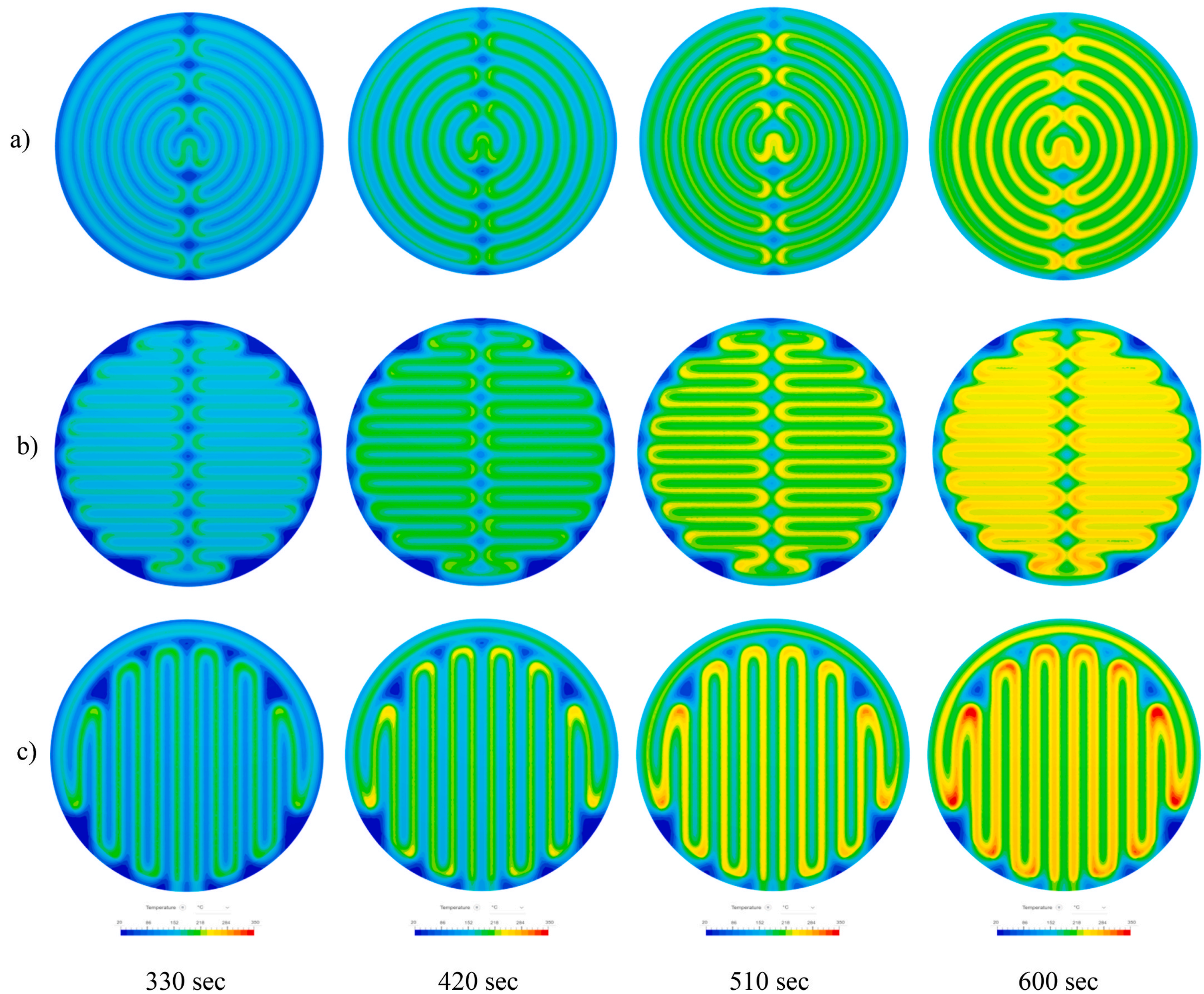

Fig. 11. Temperature distribution on the baking surface: a) model 1; b) model 2; c) model 3.

reaches the baking surface and is considered useful energy utilised for baking operations. Whereas the brown bar indicates the average heat flux value delivered to the baking plate's non-working part.

The heat flux transfer to these parts is an undesired transfer of energy. The plot shows the system heat flux transfer rate reaching equilibrium on both surfaces after 150 s of solution time. The energy performance of the system is calculated using the newly proposed performance calculation, Equation 7, using the average heat flux value recorded at 570s, system heat-up time. The system delivers a total of 827 W/m^2 of heat flux to the baking surface and 106 W/m^2 of surface heat flux delivered recorded on the non-baking surface. Therefore, using Equation 7, the heat flux ratio of the baking and non-baking surfaces of the system is calculated to be 5.3.

4.2. Proposed wiring design performance

Each subsection presents the result from the three new proposed design models.

4.2.1. Heat-up time

Fig. 10 demonstrates the temperature measurement of the baking surface of all three models. In the case of model one, Fig. 10a, all the temperature measurements show an upward trendline over time. The maximum temperature trendline has a 13.6 slope value whereas the minimum temperature recorded on the surface has a 3.51 trendline slope. The average temperature value has a 9.79 slope increment rate. In model two, the maximum, minimum and average temperature all show an increment slop value of 14.5, 0.78, and 11.3, respectively. Finally, model three, Fig. 10c, recorded 17.5, 0.64, and 11.1 slop increment rates on the maximum, minimum and average temperature on the system, respectively. The result shows that designs two and three have lower performance in delivering heat in all parts of the baking surface.

The near solution time indicates model one passes the baking temperature of 200 °C at 600s solution time, whereas the near solution from the graph indicates model two and three the average temperature at the baking surface passes the baking temperature at 540s solution time. Since the employed recording method has a 30s gap, the exact solution time that the average temperature reached the 200 °C threshold is not recorded. To fill the gap, a linear interpolation is used to calculate the result using the adjacent values and the result indicates that model two reached the threshold at 515 s, whereas model two has a startup time of 522 s.

Table 3
Summary of temperature measurement on the probe points for the proposed design.

Model 1		Temperature (°C)			
Observation points	Time step (s)	Mean	Std. Dev.	Maximum	Minimum
33	330	108	37	198	108
33	420	136	41	229	136
33	510	165	44	259	165
33	600	193	46	289	193
Model 2		Temperature (°C)			
Observation points	Time step (s)	Mean	Std. Dev.	Maximum	Minimum
33	330	116	26	153	55
33	420	151	30	192	78
33	510	187	34	230	103
33	600	223	37	269	123
Model 3		Temperature (°C)			
Observation points	Time step (s)	Mean	Std. Dev.	Maximum	Minimum
33	330	113	35	178	74
33	420	147	38	216	104
33	510	181	39	252	136
33	600	215	40	288	168

4.2.2. Temperature distribution

Fig. 11 presents the temperature distribution of all the new proposed layout designs in four-time steps. All the colour-mapped results presented in Fig. 11 have a linear temperature scale that ranges from 20 to 350 °C. The graphical heat distribution result distinctly shows the wiring layout on the baking surface as a function of temperature distribution. In configuration one, shown in Fig. 11a, the circular arrangement of the coils exhibits a total of six cold spots that are positioned on the vertical centre line of the model. The vertical line has a pitch distance of 0.03 *m* that passes at the centre, separating the round curve of the lateral coil turning points. This arrangement aided by a turning radius creates a wider gap between the coils and leads to the formation of cold spots.

Similarly, model two, illustrated in Fig. 11b, also exhibits cold spots on the vertical line passing through the centre; the main cold spots occur at the outer part of the braking surface. This is the result of the horizontal arrangement of the heating element, as it experiences a shorter length due to the circular shape of the pan and the turning radius further increases the pitch. Despite the cold and hot spots formed at the vertical centre line, the model has a genuine uniform heat distribution when compared with model one. Model three in Fig. 11c experiences cold spots in the upper section of the baking surface. The short and sharp heating element turns introduced in the design decrease the pitch distance that intensifies the hot spots formation at the outer opposing heating element vertical lines, making it the least favourite of the models under graphical inspection.

To further study the temperature uniformity quantitatively, the result at the probe point was analysed and presented in Table 3. As discussed earlier, using the measurement points in eight dominant directions from the centre of the baking surface, a total of 33 probe points were used. The temperature value at each measuring point is recorded for 32 solution steps of the transient simulation and only four solution times are presented in the table for each model. The recorded result standard deviation was calculated to determine temperature uniformity between the measuring points. A smaller deviation value indicates that the system has a uniform temperature distribution. The standard deviation calculation indicates for model one at a baking temperature solution time of 600s the temperature deviation was recorded to be 46 °C. Whereas for models two and three temperature deviations within the observed points at the respective start-up time were recorded to be 34 °C and 39 °C, respectively. From the presented result, model two has a better temperature distribution.

4.2.3. Thermal performance

As shown in the graphs presented in Fig. 12, models two and three show a slightly higher heat flux delivery to the baking surface than model one. This is related to the higher power density the system has. However, the systems also have a deficit in releasing more heat through the non-baking surface. The higher heat delivery to a non-baking surface may reduce the flux ratio of the designs. Using equation (6), the flux ratio of models one, two, and three at the respective heat-up time are 32.31, 4.17, and 5.07, respectively. And the flux ratio result shows that even though model one has the least amount of flux delivery to the baking area than the other models, the minimal heat delivery of the system to the non-baking surface has helped achieve a higher flux ratio.

5. Discussion

The new layout design follows two major design constraints. The first constraint is aimed at manufacturing and electrical work convenience, where both ends of the heating element need to start and end at the edge of the pan. Second, the layout design aims to maintain a uniform pitch distance and parallelism between adjacent parts of the heating coil across the design. To separate the coils, a pitch distance of 0.03 *m* is used for models one and two and 0.04 for model three. To avoid a sharp turn of the heating coil that could lead to heat flux concentration and lead to damage, a radius of 0.01 *m* was introduced in every corner of the design.

In general, the new designs lead to a significant reduction of contact surface area between the heating element and the baking surface when compared with the baseline design and a parametric analysis was conducted to investigate its effect on the product performance. The traditional conventional model requires the coil stretched over an 11 *m* length. Whereas, the new layout shown in Fig. 3a, b, and c has 37.1%, 32.58%, and 45.8% less length than the conventional design, respectively. This leads to an increment in the system power density as shown in Table 2. The result presented in Table 4 proves the layout design of the heating element has a direct impact on the performance of electric injera baking technology. The qualitative and quantitative examination of the four models indicates every wiring layout has its own positive and negative sides.

The conventional wiring layout has the best heat distribution from the proposed models; however, the design has the second highest heat transfer to the non-baking surface, compromising its performance. Despite model one having the highest system efficiency, it has the lowest temperature distribution on the baking surface, which threatens product quality. Further analysis of this kind opens a challenge for finding a subtle balance between the product performance parameters in the wiring layout design process. However, the basic need of the user should guide the optimization process. To identify the priority of the user, a post-analyst survey was conducted that allowed the product user to rank their prioritisation on the three-performance evaluation parameters. The survey overwhelmingly shows that uniform temperature distribution over the baking surface is highly prioritised as it relates to the quality of the baked goods. Secondly, the survey participant listed efficiency as the priority where cost-saving was mentioned as an influencing factor for the decision. The heat-up time ranked last. This prioritisation should constrain the performance optimization of the baking stove in future studies.

6. Conclusion

In this study, the impact of heat element wiring layout design on electric injera baking technology performance parameters has been investigated. For this purpose, a numerical study was employed to investigate the proposed wiring layouts and the layouts were evaluated based on impact on system efficiency, thermal distribution, and system heat-up time. The result shows that the wiring layout has a significant influence over the technical performance parameters. The heat-up time was found to be highly dependent on the heating flux surface area of the

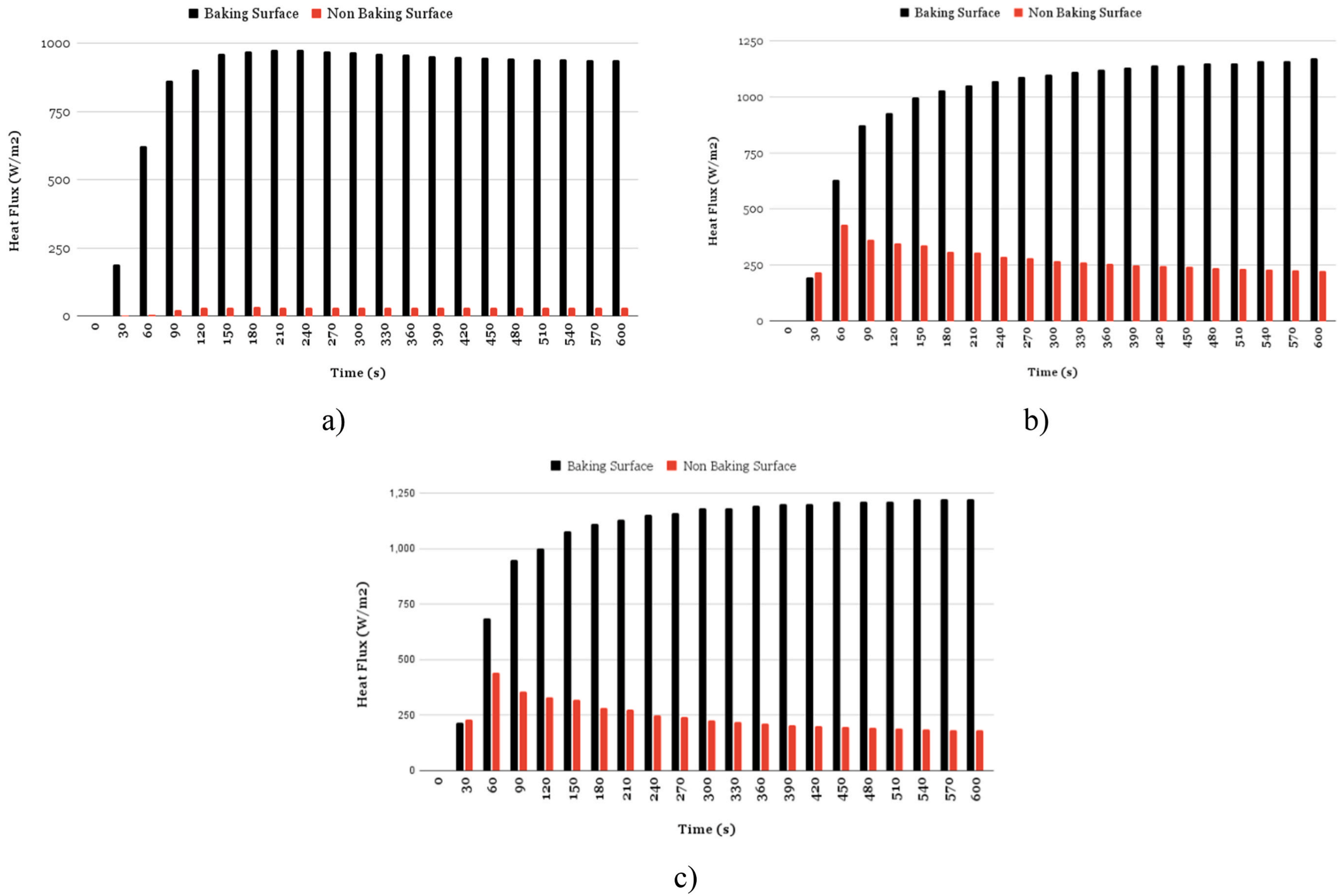

Fig. 12. Heat flux delivery to the baking surface and non-baking surface: a) model 1; b) model 2; c) model 3.

Table 4
Performance comparison.

	References baking temperature of 200 °C		Heat transfer performance				Probe point temperature distribution	
Models	Startup time (s)	Baseline comparison	Baking surface (W/m2)	Non-baking surface (W/m2)	Flux Ratio	Baseline comparison	Std. Dev.	Baseline comparison
Conventional	570	–	825	106	5.5	–	17.68	–
One	600	▼ 11%	907.10	28.07	32.31	▲ 361%	37.51	▼ 112%
Two	540	▲ 7.6%	1072.94	257.31	4.17	▼ 45%	27.95	▼ 58%
Three	522	▲ 13%	1135.80	224.01	5.07	▼ 32.4	32.12	▼ 81.6%

wiring layout. The proposed model with a lower supply heat surface area was found to achieve the heating up temperature 13% faster than the conventional model. However, this model was found to have 81% less uniformity in thermal distribution. The result also found a model with the worst thermal distribution achieved a threefold performance improvement. The result presented here clearly shows that the wiring layout has a direct effect on the performance of the baking technology. Since the baking technology has multi-performance parameters, the study of the baking technology wiring layout optimization presents property trade off challenges between the parameters. To guide future research in the field that aims to find a subtle balance between the performance parameters, the study recommends temperature distribution as the major priority followed by system efficiency and start-up time to evaluate wiring designs.

CRediT authorship contribution statement

Anwar Endris Hassen: Conceptualization, Methodology, Software, Validation, Writing - original draft, Writing - review & editing. **Lorenzo Pagliano:** Supervision, Writing - review & editing.

Declaration of competing interest

The authors declare that they have no known competing financial interests or personal relationships that could have appeared to influence the work reported in this paper.

Data availability

Data will be made available on request.

Acknowledgments

This paper and related research have been conducted during and with the support of the Italian national interuniversity PhD course in Sustainable Development and Climate Change. This paper was partially developed within the Project ABC 21 (Africa-Europe BioClimatic buildings for XXI century), which has received funding from the European Union's Horizon 2020 Research and Innovation Programme under Grant agreement no. 894712.

References

[1] IEA, World Energy Outlook 2022, IEA, Paris, 2022 [Online]. Available: https://www.iea.org/reports/world-energy-outlook-2022.
[2] J. Senyagwa, Africa Energy Outlook 2022, Jul. 2022. Accessed: Dec. 08, 2022. [Online]. Available: https://policycommons.net/artifacts/2619012/africa-energy-outlook-2022/3641723/.
[3] M.Y. Getnet, D.G. Gunjo, D.K. Sinha, Experimental investigation of thermal storage integrated indirect solar cooker with and without reflectors, Results Eng 18 (Jun. 2023), 101022, https://doi.org/10.1016/j.rineng.2023.101022.
[4] A. Mawire, K. Lentswe, P. Owusu, Performance of two solar cooking storage pots using parabolic dish solar concentrators during solar and storage cooking periods with different heating loads, Results Eng 13 (Mar. 2022), 100336, https://doi.org/10.1016/j.rineng.2022.100336.
[5] Richard Sieff, Karin Troncoso, Meron Tesfamichael, 'Ethiopia eCooking Market Assessment'. MECS and EndeV, Feb. 2022 [Online]. Available: https://mecs.org.uk/wp-content/uploads/2022/02/MECS-EnDev-Ethiopia-eCooking-Market-Assessment-presentation.pdf.
[6] A. Asfaw, Y. Demissie, Sustainable household energy for addis ababa, Ethiopia, Consilience (2012) 1–11, no. 8.
[7] Y. Alem, S. Hassen, G. Köhlin, Adoption and disadoption of electric cookstoves in urban Ethiopia: evidence from panel data, Resour. Energy Econ. 38 (2014) 110–124.
[8] Z. Gebreegziabher, A. Mekonnen, M. Kassie, G. Köhlin, Urban energy transition and technology adoption: the case of Tigrai, northern Ethiopia, Energy Econ. 34 (2) (2012) 410–418.
[9] A.H. Tesfay, M.B. Kahsay, O.J. Nydal, Design and development of solar thermal Injera baking: steam based direct baking, Energy Proc. 57 (2014) 2946–2955.
[10] R. Van Buskirk, H. Teclai, E. Negusse, The effect of clay and iron cooking plates on mogogo efficiency and energy use: experimental results, Eritrean Stud. Rev. 3 (1) (1999) 105–126.
[11] E.M. Asefa, M.T. Mergia, Human Exposure to Indoor Air Pollution in Ethiopian Households, 2022, e11528. Heliyon.
[12] T. Chen, et al., Indoor air pollution from solid fuel on children pneumonia in low- and middle-income countries: a systematic review and meta-analysis, Environ. Sci. Pollut. Res. (2022) 1–15.
[13] G.S. Downward, et al., Occupational exposure to indoor air pollution among bakery workers in Ethiopia; A comparison of electric and biomass cookstoves, Environ. Pollut. 233 (2018) 690–697.
[14] E. Flanagan, et al., Ambient and indoor air pollution exposure and adverse birth outcomes in Adama, Ethiopia, Environ. Int. 164 (2022), 107251.
[15] A. Embiale, B.S. Chandravanshi, F. Zewge, E. Sahle-Demessie, Indoor air pollution from cook-stoves during Injera baking in Ethiopia, exposure, and health risk assessment, Arch. Environ. Occup. Health 76 (2) (2021) 103–115.
[16] A.A. Hassen, D.A. Amibe, O.J. Nydal, Performance investigation of solar powered Injera Baking oven for indoor cooking, in: ISES Solar World Congress Proceedings, Kassel, Germany, 2011, pp. 186–196.
[17] K.W. Liyew, N.G. Habtu, Y. Louvet, D.D. Guta, U. Jordan, Technical design, costs, and greenhouse gas emissions of solar Injera baking stoves, Renew. Sustain. Energy Rev. 149 (Oct. 2021), 111392, https://doi.org/10.1016/j.rser.2021.111392.
[18] A. Gallagher, A solar fryer, Sol. Energy 85 (3) (Mar. 2011) 496–505, https://doi.org/10.1016/j.solener.2010.12.018.
[19] N.E. Benti, G.S. Gurmesa, T. Argaw, A.B. Aneseyee, S. Gunta, G.B. Kassahun, A. A. Asfaw, The current status, challenges and prospects of using biomass energy in Ethiopia, Biotechnology for Biofuels 14 (1) (2021) 1–24.
[20] D. Tekestebrihan, B. Yirgu, S. Demissie, Improved biogas "Injera" bakery stove design, assemble and its baking pan floor temperature distribution test, Energy Sustain. Dev. 61 (Jan. 2021) 65–73, https://doi.org/10.1016/j.esd.2020.12.009.
[21] F.M. Bayu, Cost reduction and forest preservation potential of advanced stoves and challenges of their adoption in higher education: the case of werabe university, Ethiopia, Heliyon 6 (8) (2020), e04693.
[22] A.A. Tareke, HEAT TRANSFER ANALYSIS OF INJERA BAKING PAN BY FINITE ELEMENT METHOD, 2010.
[23] P. Brinckerhoff, Ethiopian Power System Expansion Master Plan Study, Ethiopian Electric Power Corp. interim report, generation planning, 2013.
[24] EEA, 'Project document on electric Injeramitad, Energy Efficiency Standards and Labeling', Addis Ababa, Ethiopia, 2015.
[25] T.T. Awash, Experimental Investigation on Performance Characteristics and Efficiency of Electric Injera Baking Pans (MITAD), Msc Thesis, School of Postgraduate Studies, Addis Ababa University, Ethiopia, Ethiopia, 2011.
[26] R. Jones, J.C. Diehl, L. Simons, M. Verwaal, The development of an energy efficient electric Mitad for baking injeras in Ethiopia, in: 2017 International Conference on the Domestic Use of Energy (DUE), IEEE, 2017, pp. 75–82.
[27] H. Berhanu, A. Bekele, C. Venkatachalam, S. Sivalingam, Performance improvement of an electric injera baking pan (Mitad) using copper powder as additive material, Energy Sustain. Dev. 68 (2022) 242–257.
[28] A. Ayalew, Transient Heat Transfer Analysis of Injera Baking pan (" Mitad") by Finite Element Method, PhD Thesis, University of Addis Ababa, Ethiopia, 2009.
[29] G. Getenet, Heat Transfer Analysis during the Process of Injera Baking by Finite Element Method, Unpubl. Thesis Addis Ababa, 2011.
[30] A.A. Hassen, D.A. Amibe, Finite element modeling of solar powered injera baking oven for indoor cooking, J. Energy Power Eng. 7 (6) (2013) 1097.
[31] F.T. Teferi, K.P. Kolhe, Design and analytical study for influence of thermal insulation on ETHIOPIAN electric injera baking PAN (mitad), J. Eng. Sci. Technol. 16 (6) (2021) 5071–5086.

[32] J. Geng, Q. Sun, Effects of high temperature treatment on physical-thermal properties of clay, Thermochim. Acta 666 (2018) 148–155.
[33] J.R. Mehaffey, P. Cuerrier, G. Carisse, A model for predicting heat transfer through gypsum-board/wood-stud walls exposed to fire, Fire Mater. 18 (5) (Sep. 1994) 297–305, https://doi.org/10.1002/fam.810180505.
[34] J. Taler, Theory of transient experimental techniques for surface heat transfer, Int. J. Heat Mass Tran. 39 (17) (1996) 3733–3748.